A Chiral Nanohoop as Highly Efficient Asymmetric Organocatalyst

Adriana Sacristán-Martín[a]‡, Fabian Schwer[a]‡, Thomas Pickl[b], Anika Lebzelter[a], Alexander Pöthig[b], and Max von Delius[a]*

[a] Institute of Organic Chemistry, University of Ulm, Albert-Einstein-Allee 11, 89081 Ulm (Germany). Email: max.vondelius@uni-ulm.

[b] Department of Chemistry and Catalysis Research Center, Technical University of Munich (TUM), 85748 Garching b. München, (Germany)

Abstract: Chiral phosphoric acids are privileged organocatalysts that have been shown to facilitate a large variety of asymmetric transformations. In recent years, the BINOL scaffold has been equipped with large aromatic groups and transformed into dimeric imidodiphosphates to improve both chiral induction and catalyst turnover by tuning p*K*a and creating a confined space around the catalytic center. In this work, we report an alternative approach for achieving such a confinement effect within the cavity of a chiral, shape-persistent "carbon nanohoop" macrocycle. We integrated a BINOL-derived phosphoric acid into the [9]cycloparaphenylene (CPP) scaffold and employed the nanohoop as organocatalyst for the asymmetric transfer hydrogenation of quinolines. We found that the chiral macrocycle shows excellent catalytic activity with near-quantitative yields and enantioselectivities up to 96% *ee*, which is far superior to comparable non-cyclic reference catalysts. While the scope for quinolines bearing aromatic substituents is wide, we made the counterintuitive observation that the macrocyclic catalyst is not active for smaller alkyl-substituted substrates, which indicates that highly specific non-covalent effects determine the reaction outcome within the nanohoop cavity. These results suggest that outstanding selectivities can be achieved by endowing organocatalysts not only with supramolecular binding sites but also with unusual topologies.

The 2021 Nobel Prize in Chemistry has recognized the enormous potential of asymmetric organocatalysis as an environmentally benign enabling technology.[1-5] While the pioneering studies of the field were based on the reversible covalent interaction of the substrate with the catalyst (via enamine or iminium formation),[6-9] much recent work has focused on organocatalysts that interact with the substrate(s) in a non-covalent manner (e.g. thiourea catalysts).[10,11] A privileged class of catalysts that operate via non-covalent interaction are chiral BINOL (1,1'-bi-2-naphthol) phosphorus(V) Brønsted acids (Fig. 1).[12-15] Typically, these catalysts activate the substrate by protonating a Brønsted-basic nitrogen atom and subsequently coordinate the activated species by ion-pairing and/or hydrogen bonding, thus guaranteeing stereoselectivity.[14,16-18] A notable trend in BINOL-derived phosphoric acid organocatalysis is that they have been endowed with very large aromatic groups in an effort to increase stereoselectivity by generating a confined reaction space.[19-25] Similarly, two BINOL-moieties have been covalently linked in imidodiphosphates, which exhibit fine-tuned p*K*a values and highly confined reaction sites whose structural complexity resembles that found in enzyme pockets.[26]

In light of this trend toward architectures featuring confined reaction sites, we wondered whether the integration of a phosphoric acid into the cavity of a shape-persistent macrocycle could lead to improved reactivity or selectivity. The cycloparaphenylenes (CPP)[27-31] seemed particularly suitable for this purpose as they are highly strained and comprise only aromatic units, which makes them exceptionally rigid and susceptible for π-π interactions. While their optoelectronic[32,33] and supramolecular properties[29,34-38] have led to applications in organic light-emitting diodes (OLEDs),[39] organic field-effect transistors (OFET)[40] and organic photovoltaics (OPV)[41], their use in synthesis has been restricted to stoichiometric (active) template effects[42-48] and the non-specific initiation of asymmetry amplification in a Soai reaction.[49]

Herein, we report the synthesis and investigation of chiral nanohoop organocatalyst **PO$_4$H-[9]CPP**. By closing a strained CPP macrocycle around the privileged BINOL phosphoric acid, we create a unique reaction site that exhibits a well-defined cavity as well as ortho-substituents that are bent towards the cavity and conformationally restricted.[50] We chose the asymmetric transfer hydrogenation of quinolines as benchmark reaction to test the new organocatalyst, because pioneering work by Rueping established the beneficial role of large aromatic ortho-

substituents on enantioselectivity, which was attributed to a confinement effect (Fig. 1a).[19] Moreover, Niemeyer and coworkers used this reaction recently to investigate the effect of another complex topology on organocatalysis: in a highly flexible [2]catenane architecture, the interplay of two Brønsted acid sites was found to increase enantioselectivity (Fig. 1a).[51,52] We now show that the rigid nanohoop approach, despite offering only one reaction site, leads to much higher enantioselectivity than the conventional BINOL catalyst (with comparable ortho-substituents).

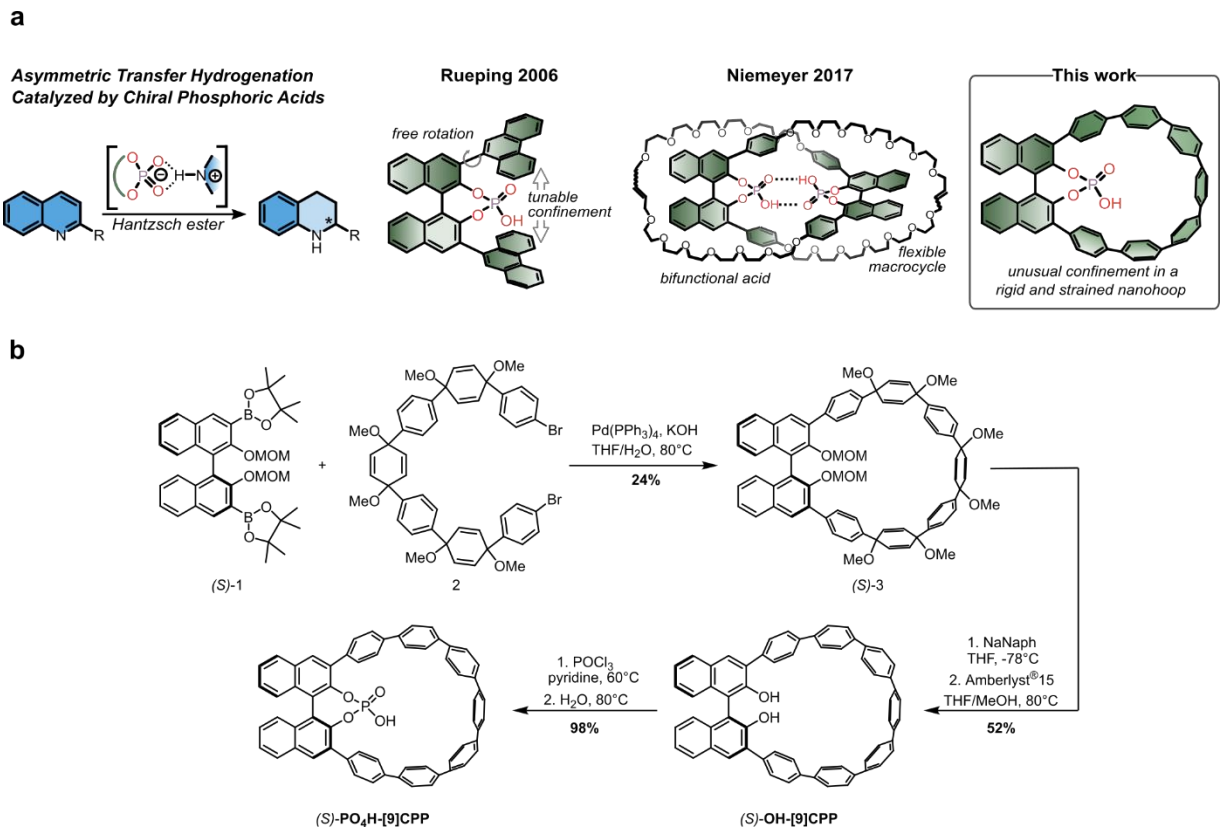

Fig. 1 | Asymmetric transfer hydrogenation of quinolines catalyzed by chiral Brønsted acids. a, Reaction scheme and relevant catalysts reported by Rueping and Niemeyer. **b**, Synthesis of nanohoop catalyst (*S*)-**PO$_4$H-[9]CPP** (MOM = methoxymethyl, NaNaph = sodium naphthalenide).

Results and discussion

Synthesis and characterization

To introduce the chiral BINOL unit into a cycloparaphenylene nanohoop, we treated enantiomerically pure MOM-protected BINOL (*S*)-**1** with dibromide **2**, a common precursor used in CPP synthesis,[32,37,53] to close the ring by Suzuki-Miyaura cross-coupling (Fig. 1b). Following the macrocyclization which proceeded in 24% yield, (*S*)-**3** was subjected to a freshly prepared solution of sodium naphthalenide to facilitate aromatization. Deprotection of the MOM groups using Amberlyst® resin produced the macrocycle (*S*)-**OH-[9]CPP** in 52% yield over two steps as a pale yellow solid. Phosphorylation of BINOL nanohoop (*S*)-**OH-[9]CPP** with $POCl_3$ with the subsequent hydrolysis of the intermediate phosphorus chloride yielded the final BINOL-derived phosphoric acid (*S*)-**PO_4H-[9]CPP** in 98% yield over the last two steps. Synthesis of the other enantiomer (*R*)-**PO_4H-[9]CPP** was performed following the same procedure from the *R*-isomer of the BINOL boronic ester (*R*)-**1** in similar yields (see S.I. for further details). All new compounds were fully characterized by ^{1}H and ^{13}C NMR spectroscopy and high-resolution mass spectrometry (Supplementary Figs. 39 – 59). Single crystals of nanohoop (*R*)-**OH-[9]CPP** were successfully grown by diffusion of *n*-hexanes into a saturated solution of the compound in 1,2-dichlorobenzene (Fig. 1). Single crystal X-ray diffraction (SC-XRD) reveals that the introduction of a BINOL moiety via *meta*-functionalization into a cycloparaphenylene results in a structure that is relatively similar to the parent nanohoop [9]CPP.[54] For instance, both (*R*)-**OH-[9]CPP** and [9]CPP exhibit, in the solid state, oval shape with near-identical internal cavity diameters of 12.8 Å (vs. 12.8 Å for [9]CPP) and 11.2 Å (vs. 11.3 Å), respectively. This structural similarity is possible because of the torsion angle of 73 ° within the BINOL skeleton, which is also responsible for the chirality of the nanohoop (Fig. 1b and Supplementary Figs. 1 - 5). Based on the Flack parameter we were able to confirm the absolute configuration of the nanohoop (*R*)-**OH-[9]CPP** in the crystal structure. In comparison to related BINOL-derived macrocycles, the new nanohoop exhibits similar structural parameters,[55-58] which is even true when comparing the BINOL torsion angle found in (*R*)-**OH-[9]CPP** with those observed in larger, less strained

nanohoops.[59] This finding indicates that the unusual catalytic activity described below are likely less due to a structurally deformed BINOL scaffold and rather due to confinement.

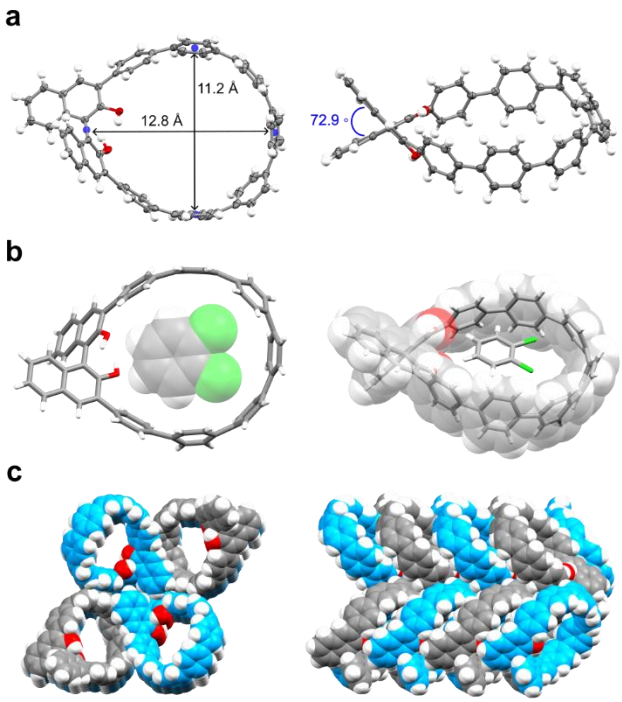

Fig. 2 | Solid state structure of (*R*)-OH-[9]CPP (SC-XRD). a, Ball-and-stick representation with key distances and BINOL torsion angle (ellipsoids shown at 50% probability; solvents omitted). **b**, Stick and space-filling representations of the same structure, showing 1,2-dichlorobenzene that co-crystallized in the cavity of the nanohoop. **c**, Molecular packing (carbon atoms are coloured blue and grey to distinguish between adjacent nanohoops).

We also carried out DFT calculations of the phosphoric acid macrocycle (*S*)-**PO$_4$H-[9]CPP** and its precursor (*S*)-**OH-[9]CPP** at the B3LYP/6–31 G(d) level of theory (for further details see the S. I.). The optimized structures of (*S*)-**PO$_4$H-[9]CPP** revealed the expected *endo* orientation of the phosphoric acid (Supplementary Fig. 6), thus creating the desired confined reaction site. The strain energy of nanohoops (*S*)-**PO$_4$H-[9]CPP** and (*S*)-**OH-[9]CPP** was determined using the homodesmotic reaction model,[62] providing nearly identical values of 40 and 42 kcal mol^{-1}, respectively. The difference in strain energy between the phosphoric acid derived nanohoop ((*S*)-**PO$_4$H-[9]CPP**) and the BINOL derived molecule ((*S*)-**OH-[9]CPP**), while relatively small, is likely real, because it is and reflected in the deviation of the BINOL torsion angle in the ring versus the relaxed geometry, which is larger for the non-tethered (*S*)-**OH-[9]CPP** macrocycle (Supplementary Fig. 6).

Catalytic performance

Having achieved the synthesis and characterization of the enantiomerically pure phosphoric acids (*S*)- and (*R*)-**PO$_4$H-[9]CPP**, we proceeded with their application in asymmetric organocatalysis. We chose the stereoselective hydrogenation of quinolines as a model reaction using the classic Hantzsch ester as a hydride donor (Table 1).[17,51,60] Our initial optimization was conducted with 2-phenylquinoline (**4a**) as substrate with (*S*)-**PO$_4$H-[9]CPP** at 10 mol% catalyst loading under conditions well-established in the literature.[51]

Table 1 | Catalyst loading and reference catalysts

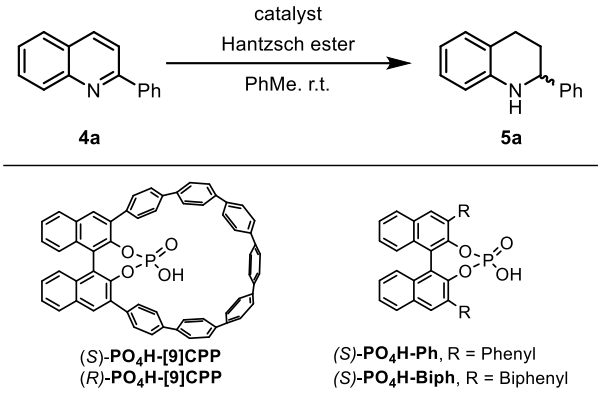

Entry	Catalyst	Cat. Loading [mol%]	Yield[a] [%]	*ee*[b] [%]
1	(*S*)-**PO$_4$H-[9]CPP**	10	88	95
2	(*S*)-**PO$_4$H-[9]CPP**	5	90	92
3	(*S*)-**PO$_4$H-[9]CPP**	2.5	89[c]	93
4	(*S*)-**PO$_4$H-Ph**	5	90	48
5	(*S*)-**PO$_4$H-Biph**	5	85	51
6	(*R*)-**PO$_4$H-[9]CPP**	5	97	-92

Reaction conditions: **4a** (5 mM), Hantzsch ester (2.4 eq), 24 h. [a] Isolated yields. [b] Determined by chiral HPLC analysis. Positive values refer to an excess of the (*R*)-enantiomer of **5a**. The absolute configuration was determined by comparison with the literature.[19] [c] Reaction was complete after 72 h.

To our delight, we observed an excellent enantioselectivity of 95% *ee*, with the (*S*) catalyst favoring the formation of the (*R*)-hydrogenated quinoline (**5a**, Table 1, entry 1). We found that decreasing the catalyst loading from 10 to 5 and 2.5 mol% did not significantly affect the

enantioselectivity or the yield of the reaction, provided that the reaction was performed over a sufficient period of time (Table 1, entry 1-3). For the remaining experiments, we opted for a catalyst loading of 5 mol% as a reasonable compromise between catalyst quantity and reaction times (typically 24 hours). We next compared our catalyst (*S*)-**PO$_4$H-[9]CPP** to the simpler BINOL derivatives (*S*)-**PO$_4$H-Ph** and (*S*)-**PO$_4$H-Biph**, which possess phenyl and biphenyl *ortho*-substituents, respectively (see Table 1). We found that the absence of a confined "pocket" in reference catalysts (*S*)-**PO$_4$H-Ph** and (*S*)-**PO$_4$H-Biph** (as an extended version, more closely resembling the constitution of the nanohoop), led to a pronounced decrease of the enantioselectivity to 48% and 51% *ee*, respectively, under otherwise identical reaction conditions (Table 1, entry 4-5). As a final experiment, we confirmed that the other enantiomer of our catalyst, (*R*)-**PO$_4$H-[9]CPP**, indeed gives rise to the (*S*)-2-phenyl-1,2,3,4-tetrahydroquinoline product ((*S*)-**5a**), which was found to be the case with the expected inverse enantioselectivity (Table 1, entry 6).

To follow up on this promising initial result, we explored the scope of the reaction with different 2-substituted quinolines (**4a-f**) (Table 2). Both the reactivity and the enantioselectivity remained at the high level observed for the phenyl derivative when using more electron-donating or electron-withdrawing aromatic substituents (Table 2, entry 2-3). The same was found for the more sterically demanding biphenyl and ^{t}butyl substituents (Table 2, entry 4-5), indicating that the nanohoop catalyst does not increase enantioselectivity at the cost of a loss of activity for larger substrates. A reasonable explanation for this result is that the catalytic site in the macrocyclic catalyst is not confined in all three dimensions, but only in two. This reasoning is in agreement with what is known about the mechanism of the reaction,[61] which features two consecutive hydrogenation events. Following the initial hydrogenation of the C−C bond, the subsequent hydrogenation of the C−N bond determines enantioselectivity. To achieve high *ee*, the Hantzsch ester needs to favour the *Re* or *Si* approach toward the complex of the substrate with the phosphate (Table 2). It is plausible that the macrocyclic architecture allows enough space for the formation of this ternary complex between catalyst, substrate and Hantzsch ester, while offering a large difference between the *Re* and *Si* face due to its exceptionally high rigidity as well as secondary π-π interactions (Table 2).[50] In contrast to the wide scope observed for aryl groups, we found that the reactivity dropped drastically when subjecting 2-alkyl-substituted quinolines

to transfer hydrogenation with our catalyst (Table 2, entry 6-7). Both 2-*n*-pentyl and 2-methyl quinolines reproducibly gave rise to sluggish reactivity and low levels of enantioselectivity, which is not the case for simple BINOL-based phosphoric acids, as reported previously by Rueping[19] and successfully reproduced by us. The observation that quinolines bearing small aliphatic groups are excellent substrates for simple catalysts, yet no good substrates for the confined nanohoop catalyst, is counterintuitive and suggests that specific non-covalent effects dictate reaction outcomes.

Table 2 | Scope study

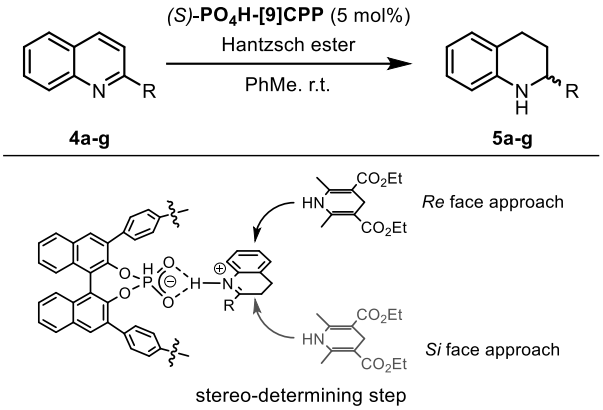

Entry	R	Yield[a][%]	*ee*[b] [%]
1	phenyl (**4a**)	quant. (90)	92
2	4-fluorophenyl (**4b**)	quant. (97)	95
3	4-methoxyphenyl (**4c**)	quant. (95)	92
4	biphenyl (**4d**)	quant. (95)	90
5	4-^{t}butylphenyl (**4e**)	quant. (88)	96
6	*n*-pentyl (**4f**)	15[c]	-20
7	methyl (**4g**)	7[d]	- 6

Reaction conditions: **4a-g** (5 mM), Hantzsch ester (2.4 eq), (*S*)-**PO4H-[9]CPP** (5 mol%), 24 h. [a] Yields determined by ^{1}H quant. NMR. Isolated yields in parentheses. [b] Determined by chiral HPLC analysis. Positive values refer to an excess of the (*R*)-enantiomer. The absolute configuration was determined by comparison with the literature.[19] [c] Yield determined by quant. HPLC after 13 days. Product not isolated. [d] Yield determined by quant. HPLC after 7 days of reaction. Product not isolated.

In an effort to gain a tentative understanding of the unexpected, low reactivity towards alkyl quinolines, we carried out several experiments. Given that the strong binding of substrate and/or product to the active catalytic site is a plausible mechanism for catalyst deactivation,[62] we tested

for “product inhibition” by performing the transfer hydrogenation of the phenyl substrate **4a** in the presence of 1 equivalent of *n*-pentyl product **5f** . After 24 hours, we observed full conversion of **4a** to the respective product **5a** with 93% *ee*, which is why we can rule out product inhibition as the origin for the low reactivity of alkyl substituted products (see further below for a study on the relative affinity of **4a**, **4f**, **5a** and **5f** for the catalyst). In a slightly different competition experiment, we combined the phenyl substrate **4a** with the *n*-pentyl substrate **4f** and observed no detectable transfer hydrogenation of **4a**, along with only 2% conversion of **4f** into **5f** after 24 hours. This experiment indicates that the presence of the alkyl substrate **4f** in the reaction medium “poisons” the catalyst for the otherwise reactive substrate **4a**, for which a possible explanation is that the alkyl substrate binds to the binding pocket with higher affinity, yet with no turnover (Supplementary Fig. 7-8). Further ^{1}H and ^{31}P NMR experiments allowed a comparison of the affinity of substrates **4a** and **4f**, as well as the hydrogenated products **5a** and **5f**, towards the catalyst (*S*)-**PO$_4$H-[9]CPP**. In sequential titration experiments between these four species, we determined that quinoline **4f** exhibited by far the highest affinity with entire affinity series being: **5a** < **4a** < **5f** < **4f** (Supplementary Fig. 9 – 14; independently corroborated by ESI-MS, see Supplementary Fig. 15– 19). Thus, the products bind less strongly to the catalyst than the substrates, which is a prerequisite for high turnover numbers in supramolecular catalysis that is easily plagued by product inhibition. The particularly strong binding of alkyl substrates to the binding pocket of the nanohoop catalyst (*S*)-**PO$_4$H-[9]CPP** however represents a problem, because it prevents catalytic turnover. At this point, we can only speculate on the specific reason is for the lack of turnover in the nanohoop cavity. A complexation-induced p*K*a shift could prevent the very first step in the catalytic cycle,[61,63] which is the protonation of the quinoline and the formation of a tightly bound ion pair, yet this seems unlikely, because alkyl-substituted quinolines are more basic than their aryl-substituted counterparts. Moreover, the structure of the ternary complex with the Hantzsch ester or its corresponding pyridine may be significantly different for alkyl substrates. However, we did not observe indications to this end in qualitative experiments focusing on the Hantzsch ester concentration and the spiking of reactions with the pyridine. Further mechanistic work on specific non-covalent effects in the nanohoop cavity is clearly needed and currently ongoing.

Optical Properties

Finally, we examined the optical and chiroptical properties of the synthesized nanohoops ((*S*)/(*R*)-**OH-[9]CPP**) (Fig. 3 and Supplementary Figs. 67 -74). The absorption spectra of (*S*)- and (*R*)-**OH-[9]CPP** exhibit a broad absorption band reaching a maximum at around 330 nm with a molar absorption coefficient of ~1.1 × 10^5 M^{-1} cm^{-1}. Both enantiomers of the nanohoop are emissive and exhibit bands with two maxima at 452 and 473 nm, which are responsible for the distinct blue emission that is typical for symmetry-broken [9]CPP-type nanohoops (Fig. 3a).[56,57,64] Electronic circular dichroism (ECD) spectra show the expected mirror-imaged spectra featuring pronounced Cotton effects thanks to the rigid conjugated architecture (Fig. 3b). The circularly polarized luminescence (CPL) spectrum of (*R*)-**OH-[9]CPP** manifests the same negative sign at higher energies as the circular dichroism spectra with a maximum of polarization at 432 nm with a g_{lum} value of -2.6·10^{-3}. (*S*)-**OH-[9]CPP** exhibits very similar and mirror shape behavior but positive g_{lum} value of +2.8·10^{-3} (Fig. 3b). Overall, the chiroptical properties fall into the useful and typical range for highly emissive conjugated macrocycles. [65,66]

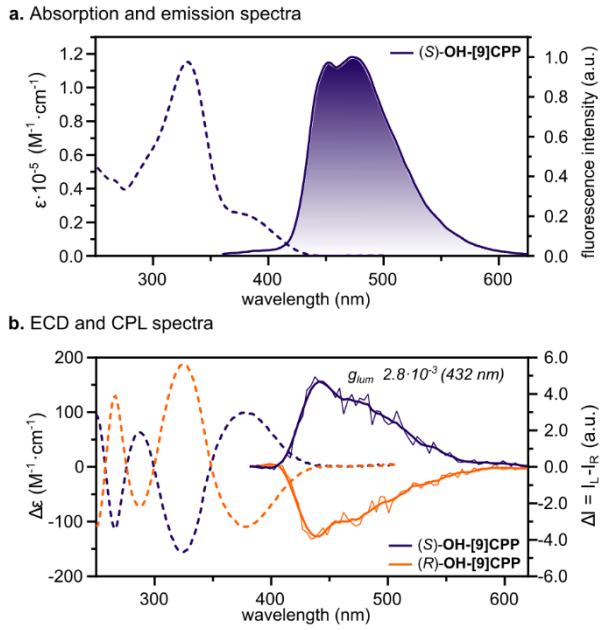

Fig. 3 | **Optical and chiroptical spectra of compounds (*S*)-OH-[9]CPP (dark purple) and (*R*)-OH-[9]CPP (orange). a**, Absorption spectrum (dashed line, CH_2Cl_2, 10^{-5} M) and emission spectrum (λ_{exc} = 330 nm, CH_2Cl_2, 10^{-7} M). **b**, Electronic circular dichroism absorption spectra (dashed lines, CH_2Cl_2, 5 ×·10^{-6} M) and circular polarized luminescence spectra (solid lines, λ_{exc} = 330 nm, CH_2Cl_2, 10^{-4} M).

Conclusion

We show that unusual selectivity and scope is observed in asymmetric transfer hydrogenations catalyzed by a BINOL phosphoric acid that is integrated into a shape-persistent CPP nanohoop. The confined and conformationally restricted reaction center leads to an increase of *ee* from ca. 50% to ca. 95% when comparing the new nanohoop organocatalyst with structurally comparable, simple BINOL phosphoric acids. While the scope for 2-aryl substituted quinolines was wide and surprisingly even included sterically rather demanding substrates, we found that 2-alkyl quinolines were not good substrates for our catalyst, which is in stark contrast to simpler catalysts that are highly effective for this type of substrates. Diverse studies on this unexpected finding point towards a highly specific effect that is due to the exceptionally strong binding of alkyl substrates to the macrocycle in conjunction with the lack of turnover. We expect that this work will inspire researchers with an interest in shape-persistent macrocycles to test compounds that are relatively easy to synthesize as catalysts. Likewise, researchers with an interest in organocatalysis may be well-advised to tackle their hardest problems with catalysts that are rigid, yet topologically non-trivial (e.g. macrocyclic,[67,68] bowl-shape,[20] cage-like,[69,70] mechanically interlocked[71]).

References

1. MacMillan, D. W. The advent and development of organocatalysis. *Nature* **455**, 304-308 (2008).
2. Schreyer, L., Properzi, R. & List, B. IDPi Catalysis. *Angew. Chem. Int. Ed.* **58**, 12761-12777 (2019).
3. Scharf, M. J. & List, B. A leap forward in the quest for general catalysts. *Nature* **610**, 632-633 (2022).
4. Brodt, N. & Niemeyer, J. Chiral organophosphates as ligands in asymmetric metal catalysis. *Org. Chem. Front.* **10**, 3080-3109 (2023).
5. García Mancheño, O. & Waser, M. Recent Developments and Trends in Asymmetric Organocatalysis. *Eur. J. Org. Chem.* **26**, e202200950 (2023).
6. Ahrendt, K. A., Borths, C. J. & MacMillan, D. W. C. New Strategies for Organic Catalysis: The First Highly Enantioselective Organocatalytic Diels−Alder Reaction. *J. Am. Chem. Soc.* **122**, 4243-4244 (2000).
7. Austin, J. F. & MacMillan, D. W. C. Enantioselective Organocatalytic Indole Alkylations. Design of a New and Highly Effective Chiral Amine for Iminium Catalysis. *J. Am. Chem. Soc.* **124**, 1172-1173 (2002).
8. List, B., Lerner, R. A. & Barbas, C. F. Proline-Catalyzed Direct Asymmetric Aldol Reactions. *J. Am. Chem. Soc.* **122**, 2395-2396 (2000).
9. List, B. The Direct Catalytic Asymmetric Three-Component Mannich Reaction. *J. Am. Chem. Soc.* **122**, 9336-9337 (2000).

10. Zhang, Z. & Schreiner, P. R. (Thio)urea organocatalysis—What can be learnt from anion recognition? *Chem. Soc. Rev.* **38**, 1187-1198 (2009).
11. Li, Q., Levi, S. M., Wagen, C. C., Wendlandt, A. E. & Jacobsen, E. N. Site-selective, stereocontrolled glycosylation of minimally protected sugars. *Nature* **608**, 74-79 (2022).
12. Uraguchi, D. & Terada, M. Chiral Brønsted Acid-Catalyzed Direct Mannich Reactions via Electrophilic Activation. *J. Am. Chem. Soc.* **126**, 5356-5357 (2004).
13. Akiyama, T., Itoh, J., Yokota, K. & Fuchibe, K. Enantioselective Mannich-Type Reaction Catalyzed by a Chiral Brønsted Acid. *Angew. Chem. Int. Ed.* **43**, 1566-1568 (2004).
14. Akiyama, T., Itoh, J. & Fuchibe, K. Recent Progress in Chiral Brønsted Acid Catalysis. *Adv. Synth. Catal.* **348**, 999-1010 (2006).
15. Terada, M. Chiral Phosphoric Acids as Versatile Catalysts for Enantioselective Transformations. *Synthesis* **2010**, 1929-1982 (2010).
16. Kampen, D., Reisinger, C. M. & List, B. Chiral Brønsted acids for asymmetric organocatalysis. *Top Curr Chem* **291**, 395-456 (2010).
17. Parmar, D., Sugiono, E., Raja, S. & Rueping, M. Complete Field Guide to Asymmetric BINOL-Phosphate Derived Brønsted Acid and Metal Catalysis: History and Classification by Mode of Activation; Brønsted Acidity, Hydrogen Bonding, Ion Pairing, and Metal Phosphates. *Chem. Rev.* **114**, 9047-9153 (2014).
18. Tsogoeva, S. B. Privileged Brønsted acid organocatalysis. *Nat. Catal.* **7**, 7-9 (2024).
19. Rueping, M., Antonchick, A. P. & Theissmann, T. A Highly Enantioselective Brønsted Acid Catalyzed Cascade Reaction: Organocatalytic Transfer Hydrogenation of Quinolines and their Application in the Synthesis of Alkaloids. *Angew. Chem. Int. Ed.* **45**, 3683-3686 (2006).
20. Mitschke, B., Turberg, M. & List, B. Confinement as a Unifying Element in Selective Catalysis. *Chem* **6**, 2515-2532 (2020).
21. Gramage-Doria, R. & Reek, J. N. H. Organocatalysis in Confined Spaces. *ChemCatChem* **5**, 677-679 (2013).
22. Berkessel, A. & Gröger, H. *Asymmetric Organocatalysis* (Wiley-VCH Verlag GmbH & Co. KGaA, 2005).
23. Pellissier, h. Recent Developments in Asymmetric Organocatalysis. *RSC Catalysis Series*, 1-258 (2010).
24. Kuil, M., Soltner, T., van Leeuwen, P. W. N. M. & Reek, J. N. H. High-Precision Catalysts: Regioselective Hydroformylation of Internal Alkenes by Encapsulated Rhodium Complexes. *J. Am. Chem. Soc.* **128**, 11344-11345 (2006).
25. Cavarzan, A., Scarso, A., Sgarbossa, P., Strukul, G. & Reek, J. N. H. Supramolecular Control on Chemo- and Regioselectivity via Encapsulation of (NHC)-Au Catalyst within a Hexameric Self-Assembled Host. *J. Am. Chem. Soc.* **133**, 2848-2851 (2011).
26. Schwengers, S. A. *et al.* Unified Approach to Imidodiphosphate-Type Brønsted Acids with Tunable Confinement and Acidity. *J. Am. Chem. Soc.* **143**, 14835-14844 (2021).
27. Darzi, E. R. & Jasti, R. The dynamic, size-dependent properties of [5]–[12]cycloparaphenylenes. *Chem. Soc. Rev.* **44**, 6401-6410 (2015).
28. Lewis, S. E. Cycloparaphenylenes and related nanohoops. *Chem. Soc. Rev.* **44**, 2221-2304 (2015).

29. Xu, Y. & von Delius, M. The Supramolecular Chemistry of Strained Carbon Nanohoops. *Angew. Chem. Int. Ed.* **59**, 559-573 (2020).
30. Wang, J., Zhang, X., Jia, H., Wang, S. & Du, P. Large π-Extended and Curved Carbon Nanorings as Carbon Nanotube Segments. *Acc. Chem. Res.* **54**, 4178-4190 (2021).
31. Krasley, A. T. *et al.* Carbon Nanomaterial Fluorescent Probes and Their Biological Applications. *Chem. Rev.* (2024).
32. Huang, Q. *et al.* Photoconductive Curved-Nanographene/Fullerene Supramolecular Heterojunctions. *Angew. Chem. Int. Ed.* **58**, 6244-6249 (2019).
33. Leonhardt, E. J. & Jasti, R. Emerging applications of carbon nanohoops. *Nat. Rev. Chem.* **3**, 672-686 (2019).
34. Iwamoto, T., Watanabe, Y., Sadahiro, T., Haino, T. & Yamago, S. Size-Selective Encapsulation of C60 by [10]Cycloparaphenylene: Formation of the Shortest Fullerene-Peapod. *Angew. Chem. Int. Ed.* **50**, 8342-8344 (2011).
35. Wu, D., Cheng, W., Ban, X. & Xia, J. Cycloparaphenylenes (CPPs): An Overview of Synthesis, Properties, and Potential Applications. *Asian J. Org. Chem.* **7**, 2161-2181 (2018).
36. Lu, D. *et al.* The Supramolecular Chemistry of Cycloparaphenylenes and Their Analogs. *Front. Chem.* **7** (2019).
37. Schwer, F. *et al.* Synthesis and C60 Binding of Aza[10]CPP and N-Methylaza[10]CPP. *Organic Materials* **4**, 7-17 (2022).
38. Stasyuk, O. A., Voityuk, A. A., Stasyuk, A. J. & Solà, M. Photoinduced Electron Transfer in Inclusion Complexes of Carbon Nanohoops. *Acc. Chem. Res.* (2023).
39. Roy, R., Brouillac, C., Jacques, E., Quinton, C. & Poriel, C. π-Conjugated Nanohoops: A New Generation of Curved Materials for Organic Electronics. *Angew. Chem. Int. Ed.* **63**, e202402608 (2024).
40. Lucas, F. *et al.* Electronic and Charge Transport Properties in Bridged versus Unbridged Nanohoops: Role of the Nanohoop Size. *Chem. Eur. J.* **29**, e202300934 (2023).
41. Della Sala, P. *et al.* An Anthracene-Incorporated [8]Cycloparaphenylene Derivative as an Emitter in Photon Upconversion. *J. Org. Chem.* **83**, 220-227 (2018).
42. Xu, Y. *et al.* Concave-Convex π-π Template Approach Enables the Synthesis of [10]Cycloparaphenylene-Fullerene [2]Rotaxanes. *J Am Chem Soc* **140**, 13413-13420 (2018).
43. Ubasart, E. *et al.* A three-shell supramolecular complex enables the symmetry-mismatched chemo- and regioselective bis-functionalization of C60. *Nat. Chem.* **13**, 420-427 (2021).
44. Steudel, F. M. *et al.* Synthesis of C60/[10]CPP-Catenanes by Regioselective, Nanocapsule-Templated Bingel Bis-Addition. *Angew. Chem. Int. Ed.* **n/a**, e202309393 (2023).
45. Iannace, V. *et al.* Regioswitchable Bingel Bis-Functionalization of Fullerene C70 via Supramolecular Masks. *J. Am. Chem. Soc.* **146**, 5186-5194 (2024).
46. Van Raden, J. M., White, B. M., Zakharov, L. N. & Jasti, R. Nanohoop Rotaxanes from Active Metal Template Syntheses and Their Potential in Sensing Applications. *Angew. Chem. Int. Ed.* **58**, 7341-7345 (2019).

47. May, J. H., Van Raden, J. M., Maust, R. L., Zakharov, L. N. & Jasti, R. Active template strategy for the preparation of pi-conjugated interlocked nanocarbons. *Nat Chem* **15**, 170-176 (2023).
48. May, J. H., Fehr, J. M., Lorenz, J. C., Zakharov, L. N. & Jasti, R. A High-Yielding Active Template Click Reaction (AT-CuAAC) for the Synthesis of Mechanically Interlocked Nanohoops. *Angew. Chem. Int. Ed.* **63**, e202401823 (2024).
49. Hitosugi, S. *et al.* Asymmetric Autocatalysis Initiated by Finite Single-Wall Carbon Nanotube Molecules with Helical Chirality. *Org. Lett.* **16**, 645-647 (2014).
50. Grommet, A. B., Feller, M. & Klajn, R. Chemical reactivity under nanoconfinement. *Nat. Nanotechnol.* **15**, 256-271 (2020).
51. Mitra, R., Zhu, H., Grimme, S. & Niemeyer, J. Functional Mechanically Interlocked Molecules: Asymmetric Organocatalysis with a Catenated Bifunctional Brønsted Acid. *Angew. Chem. Int. Ed.* **56**, 11456-11459 (2017).
52. Jansen, D. *et al.* What is the role of acid–acid interactions in asymmetric phosphoric acid organocatalysis? A detailed mechanistic study using interlocked and non-interlocked catalysts. *Chem. Sci.* **11**, 4381-4390 (2020).
53. Wassy, D. *et al.* Enantiopure nanohoops through racemic resolution of diketo[n]CPPs by chiral derivatization as precursors to DBP[n]CPPs. *Chem. Sci.* **12**, 10150-10158 (2021).
54. Segawa, Y., Šenel, P., Matsuura, S., Omachi, H. & Itami, K. [9]Cycloparaphenylene: Nickel-mediated Synthesis and Crystal Structure. *Chem. Lett.* **40**, 423-425 (2011).
55. Malinčík, J. *et al.* Circularly Polarized Luminescence in a Möbius Helicene Carbon Nanohoop. *Angew. Chem. Int. Ed.* **61**, e202208591 (2022).
56. Sato, K. *et al.* Circularly Polarized Luminescence of a Stereogenic Curved Paraphenylene Anchoring a Chiral Binaphthyl in Solution and Solid State. *Chem. Eur. J.* **27**, 1323-1329 (2021).
57. Huang, Q. *et al.* Binaphthyl-derived armchair-type molecular carbon rings with chirality: synthesis and optical properties. *Org. Chem. Front.* **10**, 911-915 (2023).
58. Yu, Y. *et al.* BINOL-Based Chiral Macrocycles and Cages. *Angew. Chem. Int. Ed.* **63**, e202407034 (2024).
59. Fang, P., Chen, M., Zhang, X. & Du, P. Selective synthesis and (chir)optical properties of binaphthyl-based chiral carbon macrocycles. *Chem. Commun.* **58**, 8278-8281 (2022).
60. Thiele, M. *et al.* Multifunctional Organocatalysts - Singly-Linked and Macrocyclic Bisphosphoric Acids for Asymmetric Phase-Transfer and Brønsted-Acid Catalysis. *Chem. Eur. J.* **29**, e202202953 (2023).
61. Pastor, J. *et al.* Revised Theoretical Model on Enantiocontrol in Phosphoric Acid Catalyzed H-Transfer Hydrogenation of Quinoline. *J. Org. Chem.* **83**, 2779-2787 (2018).
62. Ballester, P. & Vidal-Ferran, A. in *Supramolecular Catalysis* Ch. 1, (WILEY-VCH Verlag GmbH & Co. KGaA, 2008).
63. Kim, H. *et al.* Role of Ion-Pairs in Brønsted Acid Catalysis. *ACS Catalysis* **5**, 6630-6633 (2015).
64. Lovell, T. C., Colwell, C. E., Zakharov, Lev N. & Jasti, R. Symmetry breaking and the turn-on fluorescence of small, highly strained carbon nanohoops. *Chem. Sci.* **10**, 3786-3790 (2019).

65. Tanaka, H., Inoue, Y. & Mori, T. Circularly Polarized Luminescence and Circular Dichroisms in Small Organic Molecules: Correlation between Excitation and Emission Dissymmetry Factors. *ChemPhotoChem* **2**, 386-402 (2018).
66. Hasegawa, M. & Mazaki, Y. Stereogenic π-Conjugated Macrocycles: Synthesis, Structure, and Chiroptical Properties Including Circularly Polarized Luminescence. *Synlett* (2023).
67. Wang, C., Xu, L., Jia, Z. & Loh, T.-P. Recent applications of macrocycles in supramolecular catalysis. *Chin. Chem. Lett.* **35**, 109075 (2024).
68. Schulze, M., Kunz, V., Frischmann, P. D. & Würthner, F. A supramolecular ruthenium macrocycle with high catalytic activity for water oxidation that mechanistically mimics photosystem II. *Nat. Chem.* **8**, 576-583 (2016).
69. Piskorz, T. K., Martí-Centelles, V., Spicer, R. L., Duarte, F. & Lusby, P. J. Picking the lock of coordination cage catalysis. *Chem. Sci.* **14**, 11300-11331 (2023).
70. Li, T.-R., Huck, F., Piccini, G. & Tiefenbacher, K. Mimicry of the proton wire mechanism of enzymes inside a supramolecular capsule enables β-selective O-glycosylations. *Nat. Chem.* **14**, 985-994 (2022).
71. Kwamen, C. & Niemeyer, J. Functional Rotaxanes in Catalysis. *Chem. Eur. J.* **27**, 175-186 (2021).

Methods

Experimental methods

Synthesis of (*S*)-3

Under N_2, (*S*)-**1** (0.36 g, 0.57 mmol, 1.0 equiv), **2** (0.50 g, 0.57 mmol, 1.0 equiv), $Pd(PPh_3)_4$ (33 mg, 0.03 mmol, 0.05 equiv) and KOH (0.16 g, 2.85 mmol, 5.0 equiv) were suspended in a degassed mixture of THF (225 ml) and water (25 mL). The mixture was stirred for 16 h at 80 °C. THF was removed under reduced pressure, water was added, and the mixture was extracted three times with DCM. The combined organic phases were dried over $MgSO_4$ and concentrated under reduced pressure. The crude product was purified by column chromatography (cyclohexane / ethyl acetate 95:5 → 60:40) to yield (*S*)-**3** as colourless solid (0.15 g, 0.14 mmol, 24%).

Synthesis of (*S*)-OH-[9]CPP

Under N_2, naphthalene (1.28 g, 10.0 mmol, 1.0 equiv) was dissolved in anhydrous THF (20 mL). Small pieces of sodium metal (342 mg, 15.0 mmol, 1.5 equiv) was added to the solution which was stirred for 16 h at room temperature yielding sodium naphthalenide as dark green solution. Under N_2, (*S*)-**3** (0.14 g, 0.13 mmol, 1.0 equiv) was dissolved in anhydrous THF (10 mL) and

cooled down to -78 °C. The freshly prepared solution of sodium naphthalenide (3.0 mL, 0.5 M, 1.50 mmol, 12 equiv) was added dropwise and the solution stirred at -78 °C for further 2 h. The reaction was quenched by adding a solution of iodine in THF. An aqueous solution of $Na_2S_2O_3$ was added and the reaction was extracted with DCM and the combined organic layers were dried over $MgSO_4$ and concentrated under reduced pressure. The crude product was then dissolved in anhydrous THF (20 mL) and methanol (10 mL) and stirred for 1 d at 70 °C together with Amberlyst® 15 (0.20 g). After cooling down to room temperature, Amberlyst® 15 was filtered of, the solution was concentrated under reduced pressure and purified by column chromatography (petroleum ether / DCM 3:2 → 1:1) to yield (*S*)-**OH-[9]CPP** as yellow solid (54 mg, 66 µmol, 52%).

Synthesis of (*S*)-PO_4H-[9]CPP

Under N2, (*S*)-**OH-[9]CPP** (20 mg, 24 µmol, 1.0 equiv) was dissolved in anhydrous pyridine (2 mL). $POCl_3$ (18.7 mg, 12 µL, 0.12 mmol, 5.0 equiv) was added to the solution and the mixture was heated at 60 °C during 24 h. After that time, H_2O (2 mL) was added and heated at 60 °C for another 24 h. Then, the reaction was allowed to cool down to r.t. and the solvent was evaporated under reduced pressure. The crude was extracted three times with DCM using HCl (3 M) as aqueous phase and the combined organic layers were concentrated under reduced pressure without drying the organic phase. The resulting yellow solid was repeatedly washed with toluene in order to remove any traces of HCl and evaporated under reduced pressure to co-evaporate with the remaining traces of water. Final compound (*S*)-**PO_4H-[9]CPP** was recovered as a light yellow solid (20 mg, 23 µmol, 98%).

General procedure for organocatalytic transfer hydrogenations

Under N_2, quinoline **4a-g** (25 µmol, 1.0 equiv), 1,4-dihydro-2,6-dimethyl-3,5-pyridinedicarboxylic acid diethyl ester (60 µmol, 2.4 equiv) and organocatalyst were dissolved in anhydrous toluene (5 mL). The reaction was stirred at room temperature and monitored by TLC. When TLC indicated full consumption of the starting material, the solvent was evaporated under reduced pressure and the crude product was purified by flash chromatography (cyclohexane / ethyl acetate 100:0 → 90:10).

Data availability

Detailed synthesis and catalysis procedures, crystallography data of (*R*)-**OH-[9]CPP**, HPLC traces, DFT analysis, computational calculation details, characterization by 1D NMR along with HR-MS spectra, UV−vis absorption and emission experiment details including CD and CPL spectra (PDF).

Acknowledgments

The authors acknowledge financial support by the Deutsche Forschungsgemeinschaft (DFG) project numbers 182849149 SFB 953 “Synthetic Carbon Allotropes”, 364549901 SFB TRR 234 “CataLight” and infrastructure provided by the state of Baden-Württemberg through bwHPC and the DFG through grant no. INST 40/575–1 FUGG (JUSTUS 2 cluster). A.S.M thanks the Ramon Areces Foundation for a postdoctoral fellowship.

Author Contributions

‡These authors contributed equally. A.S.M. and F.S. performed the synthesis and characterization of all compounds as well as the catalysis experiments and analyzed the results with M.v.D. A.S.M. and F.S. wrote the initial draft of the manuscript. T.P. and A.P. gathered the data and solved the SCXRD structure of (*R*)-**OH-[9]CPP**. A.L. performed the catalyst synthesis at an early stage of the project. M.v.D. conceived the project idea and wrote the final manuscript. All authors contributed to the discussion and the preparation of the manuscript.

Competing interest

The authors declare no competing interests.